frontiers | Frontiers in Earth Science

TYPE Original Research
PUBLISHED 04 August 2022
DOI 10.3389/feart.2022.954547

Check for updates

OPEN ACCESS

EDITED BY
Guang-Liang Feng,
Institute of Rock and Soil Mechanics (CAS), China

REVIEWED BY
Liu Liu,
Institute of Rock and Soil Mechanics (CAS), China
Qiu Enxi,
Southwest Petroleum University, China

*CORRESPONDENCE
Zhang Jun,
zhangjun07@tyut.edu.cn

SPECIALTY SECTION
This article was submitted to Geohazards and Georisks, a section of the journal Frontiers in Earth Science

RECEIVED 27 May 2022
ACCEPTED 27 June 2022
PUBLISHED 04 August 2022

CITATION
Jun Z, Yiliang W, Liming C, Ning W, Yuepin B and Chaofan W (2022), Workspace analysis and motion control strategy of robotic mine anchor drilling truck manipulator based on the WOA-FOPID algorithm.
Front. Earth Sci. 10:954547.
doi: 10.3389/feart.2022.954547

COPYRIGHT
© 2022 Jun, Yiliang, Liming, Ning, Yuepin and Chaofan. This is an open-access article distributed under the terms of the Creative Commons Attribution License (CC BY). The use, distribution or reproduction in other forums is permitted, provided the original author(s) and the copyright owner(s) are credited and that the original publication in this journal is cited, in accordance with accepted academic practice. No use, distribution or reproduction is permitted which does not comply with these terms.

Workspace analysis and motion control strategy of robotic mine anchor drilling truck manipulator based on the WOA-FOPID algorithm

Zhang Jun[1,2,3]*, Wang Yiliang[1], Che Liming[2,4], Wang Ning[5], Bai Yuepin[5] and Wang Chaofan[1]

[1]School of Mechanical and Transportation Engineering, Taiyuan University of Technology, Taiyuan, China, [2]China Coal Science and Industry Group Co., Ltd., Beijing, China, [3]Ningxia Tiandi Benniu Industrial Group Co, Ltd., Shizuishan, China, [4]Taiyuan Research Institute of China Coal Science and Industry Group, Taiyuan, China, [5]Shanghai Research Institute of China Coal Science and Industry Group, Shanghai, China

The manipulator is the key component of the anchor drilling robot to automatically complete the anchoring operation underground. Due to the complexity of its motion equation and the limitations of its control strategy, the real-time pose and the positioning accuracy of the manipulator are inferior, which seriously restricts the safety, efficiency, and speed of roadway excavation. In order to improve the positioning accuracy and realize the optimal efficiency of the manipulator, this article designs a manipulator structure with four degrees of freedom. With the help of the D-H method and the intelligent parameter setting method, this article carries out the basic theoretical research on the kinematics and the fractional order FOPID control algorithm of the manipulator of the mining roof bolter, and formulates a manipulator motion control strategy. At the same time, combined with numerical simulations and field experiments, we explore the robustness and control efficiency of the hydraulic system of the manipulator under the working conditions of a harsh environment and limited space, and reveal that the intelligent optimization algorithm can control the motion state of the manipulator more accurately and stably after the parameters of the fractional order FOPID controller are positively determined. This study effectively solved the dynamic model uncertainty caused by time-varying internal parameters and external loads of the hydraulic servo system, optimized and reconstructed the structure and motion coefficient parameters of the manipulator, and revealed the control mechanism of a precise spatial positioning and online trajectory planning of the hydraulic servo system of the manipulator. Compared with the traditional PID control algorithm, this algorithm has a faster response speed and better expected track tracking ability. This research lays a theoretical foundation for the precise positioning and automatic support of the manipulator, and also provides a reference for the design of similar motion control algorithms.

KEYWORDS
manipulator, fractional FOPID, whale algorithm, motion control, anchor drilling robot

1 Introduction

The intellectualization of coal mines is the core technical support for the high-quality development of China's coal industry (Wang et al., 2019; Liu et al., 2021). Intelligent equipment and support technology of mining are key factors for coal intellectualization, and the roadway support theory and technology have always been the core of the coal mine strata control (Kang, 2007; Wang et al., 2018; Wang et al., 2020; Yang et al., 2022). In the "Catalog of Key Research and Development of Coal Mine Robots" (Author Anonymous, 2019; Li et al., 2019; Ge and Hu, 2020), it clearly points out the need to vigorously advance the research and development of coal mining, tunneling, transportation, safety control and rescue, and 38 kinds of coal mine robots, which is an important way to achieve the coal mines' intellectualization. It is a key method to solve the problems of roadway excavation, support imbalance and high labor intensity to use the manipulator of anchor drilling robot on accurate location, and the completion of the automatic anchoring work, replacing the traditional manual completion of automatic positioning and support work of the drilling frame (Zhang et al., 2019; Zhang and Li, 2019).

Compared with developed countries, the ineffective bolt support in some coal mines in China has led to many roof falling accidents. While the main reason is that the existing support operations still rely on manual demolition, with the installation of drill pipes or bolts, bolt fastening, and other processes, with a great danger. The Guiding Opinions on Accelerating the Intelligent Development of Coal Mines clearly points out that the development of an anchor drilling support robot is an effective way to solve the key problems of slow speed and high labor intensity of roadway excavation.

Based on the guidance of the support theory, the bottleneck problem to be solved is to complete the automatic anchoring work with the use of an anchor drilling manipulator for precise positioning, replacing the traditional manual to complete of the drilling frame space positioning, and automatic support work. Since presently, the drivage speed and coal quantity have increases, so new requirements have been put forward for the way of the operation, process time, and the safety of the anchor drilling manipulator. Especially in harsh or limited spaces, manipulator ends need to accurately find the 22 mm diameter hole in the roof, effectively avoid the grid reinforced at the same time, and ensure that the drilling time does not exceed 3 min. However, in the process of drilling and anchoring by a manipulator-replacing manual operation, due to limitations in the formulation of control strategy, the real-time pose and positioning accuracy of the manipulator are inferior, essentially because the research studies are not sufficient in the fields of structural design, motion law, and control mechanism of the anchor drilling manipulator.

In recent years, the way to control the motion of the manipulator is a research hotspot with great significance. Because of its uncertainties in parameter uptake and external interference, the manipulator is a complex research object featuring high non-linearity, multi-variability, and high coupling. In order to make the manipulator in a specific action, it is necessary to control the hydraulic cylinder and hydraulic motor at each joint of the manipulator to cooperate with each other to complete the corresponding rotation angle of each joint. Presently, the manipulator structure has become increasingly complex, and the *PID* control method, with characteristics of independence on the system model, simple and flexible, is unable to meet the motion control of the current manipulator's complex structure. In view of this practical need, many experts and scholars put forward some new methods based on the idea of control. For example, Chen Wei et al. (Chen et al., 2013) adopted the control method and designed the control algorithm of active and passive joints respectively, realized the underactuated manipulator with passive joints and flexible bars in a piecewise control, and the active and passive joints could effectively complete the operation tasks of the manipulator through the control method. Li et al. (Li and Xing, 2007) studied the skid situation of the left and right tracks of the underwater robot under the complex damping coupling action, and established a *PID* control model for automatic tracking of the predetermined mining path with ADAMS/Hydraulics and MATLAB/Simulink, which confirmed that the maximum skid rate of the underwater robot in China was 15%. Jing Xuedong et al. (Jing and Pan, 2018) adopted the switch structure control method with acceleration feedback to improve the positioning accuracy of the manipulator. Compared with the traditional *PID* control method, the fuzzy *PID* control system has more advantages in overshoot and reaction speed. Zhang Tiemin (Zhang et al., 2002) et al. used the switch structure control method with acceleration feedback to reduce the vibration amplitude to 1/10 of the *PID* control method and shorten the vibration attenuation time. Luo Yanlei (Luo et al., 2021) et al. established a model on the basis of MATLAB and the AMEsim software and designed a system method of fuzzy *PID* controller, adopted fuzzy *PID* controller strategy, which has increased the accuracy and working speed of the hydraulic blanking machine, and has advantages of a strong tracking ability and good robustness. However, in some special conditions, to quickly achieve the goal of spatial positioning and trajectory tracking with the manipulator, the effect of a traditional *PID* control is not ideal, as the expected control goal is still not achieved even if the parameters are reset. Since the defects of integer order *PID* control technology cannot be overcome in essence, it is difficult

to thoroughly develop the control principle of a fast and accurate spatial positioning and trajectory planning of the manipulator control system. To sum up, in the process of realizing the control of the multi-degree of the freedom electro-hydraulic servo manipulator, a series of problems of complicated mechanisms, motion characteristics, hydraulic servo drive non-linear, feedback control characteristics, and energy characteristics, are critical points to fulfill the precision, stability, and efficiency of the motion control of the anchor drilling manipulator.

With the gradual development of artificial intelligence technology and its wide application in the industrial field, a large number of efficient optimization algorithms have emerged, such as the genetic algorithm (Zhang et al., 2002; Yin et al., 2014a; Luo et al., 2021), particle swarm optimization algorithm (Feng et al., 2015; Al-Saggaf et al., 2020; Feng et al., 2022), search algorithm (Wu and Huang, 2021), and whale algorithm (Li et al., 2021). Applying the intelligent optimization algorithm to controller parameter tuning can greatly improve the control effect. Whale algorithm is a kind of meta-heuristic optimization algorithm, which has the characteristics of strong robustness, simple structure, and few control parameters. Most scholars (Dalir and Bigdeli, 2020; Bushnaq et al., 2021; Nguyen et al., 2021) have applied the whale algorithm and achieved successful examples in the field of continuous domain problem optimization.

To sum up, many experts have conducted in-depth research studies on the method of the intelligent control PID parameter adjustment and achieved a lot of results, but the control method of the drilling and anchor manipulator completing automatic support operation underground needs further research. This is mainly due to some particularity of the drilling and anchoring manipulator working underground: 1) limited space and a complex environment; 2) The end of the anchor drilling mechanical arm is mainly connected with the automatic drill frame. Due to the dead weight of the end and the drilling force of about 20,000 n, the arm end will vibrate greatly, making it difficult to achieve accurate control; 3) Underground electrical parts need explosion-prevention treatment, especially sensors. Compared with sensors on the ground, many performance indicators are difficult to achieve, so it will affect the accurate positioning of the drilling and anchoring manipulator in the roadway space. It seriously restricts the application of intelligent control technology in an underground coal mine robot.

In order to realize the goal of rapid spatial positioning and trajectory tracking of the manipulator, the intelligent control technology of the drilling anchor manipulator is studied. According to the spinor theory, the joint coordinate system and coordinate transformation matrix expression of the manipulator are established by using the D–H method, and the point cloud diagram of the manipulator workspace is solved by using the Monte Carlo algorithm. Based on the independent joint control theory, the single input single output system model of the hydraulic motor/cylinder at the joint of the manipulator is designed by using the MATLAB Simulink software and fractional order FOPID control technology. This article analyzes four intelligent optimization algorithms based on the genetic algorithm (GA), particle swarm optimization (PSO), whale algorithm (WOA), and search algorithm (GPS), evaluates the three dynamic indexes of standard deviation, overshoot, and stability time, and analyzes the effect of step influence under different control combination strategies of the hydraulic motor/oil cylinder. The simulation results show that the optimization ability of the *WOA* algorithm is obvious. For the fractional order controlled object, it can be stable in 0.19 s, and the overshoot is 3.49%, which shows that the controlled system has better stability and fully reflects the advantages of the *FOPID* fractional order controller. Finally, the design and experiment are carried out combined with the manipulator control system of the anchor drilling robot.

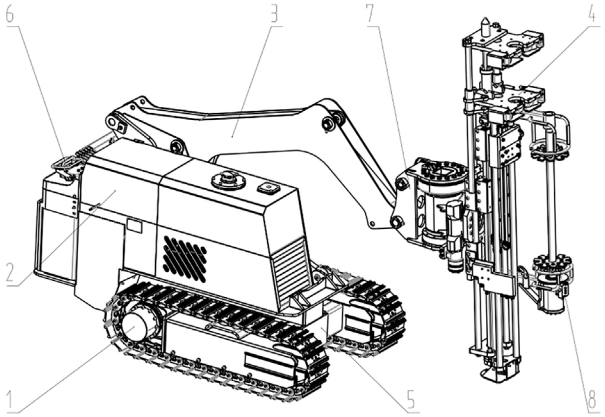

FIGURE 1
Structural diagram of the mine anchor drill frame.

2 Structural design and working principle of the manipulator

Mining roof bolter is suitable for automatic support of the top and side walls of the mine tunnel in an underground coal mine, and can realize accurate identification and positioning technology of the manipulator hole location through binocular stereo vision. The structure of the machine is shown in Figure 1. The manipulator connected the frame with the translation pair and the rotation pair realizes the support work of the automatic drilling frame, and ensures the support work of the top and side walls of the roadway with different heights and widths in the mine environment.

1-Variable frequency speed-regulating traveling mechanism, 2-Electrical control system, 3-Connecting rod, 4-Automatic drill

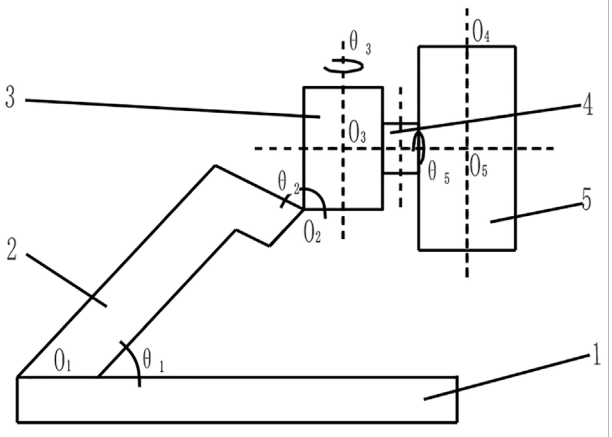

FIGURE 2
Structure diagram of the manipulator.

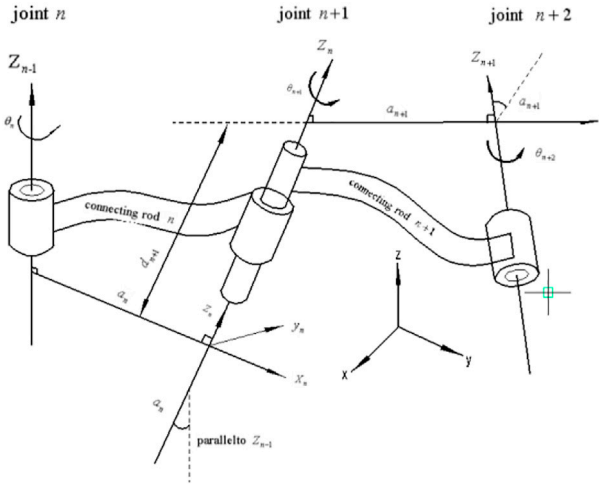

FIGURE 3
Schematic diagram of the *D* – *H* model.

frame, 5-Frame, 6-Driving operation and monitoring mechanism, 7-Rotary reducer, 8-Anchor rod silo.

During mining roof bolter into the mine roadway, firstly, it is driven to the work scheduled area, after being stable, the manipulator controlled by the hydraulic system to automatically drill stands up to the right height through the rotary gear reducer to adjust the automatic drill's stand posture. Then, the automatic drill starts to work on the working surface, and finally completes the mine roadway support work.

3 Kinematic workspace analysis of the manipulator

The manipulator is the main working structure of the equipment to realize the automatic support of the top and side walls of the roadway. The positioning system of the manipulator is the important factor to ensure that mining roof bolter can meets the working requirements and work quality. It is required that the displacement working accuracy offset of the manipulator shall not be more than 5 mm, and the displacement working accuracy offset of the manipulator end shall not be more than 10 mm. In addition, as the bad environment in the mine roadway, frequent vibration, and changeable load, a manipulator structure with five degrees of freedom is specially designed to meet the actual requirements of the aforementioned working process. The manipulator is mainly composed of a connecting rod, rotary reducer, coupling, automatic drilling frame, and so on. Its structural diagram is shown in Figure 2.

1 - Frame; 2 - Connecting rod; 3 - Rotary reducer; 4 - Connection shaft; 5-Automatic drilling rig.

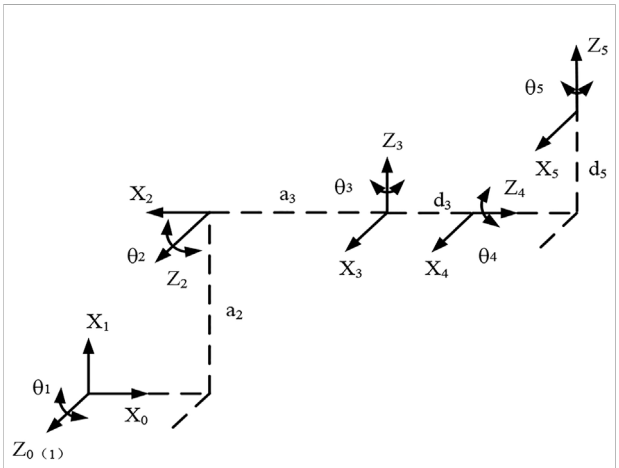

FIGURE 4
Establishment of a joint coordinate system of the manipulator by using the *D* – *H* method.

The frame is set at the lower end of the whole manipulator as the main body supporting the whole manipulator; the connecting rod is connected through the shaft, and the hydraulic cylinder provides power which can rotate θ_1 around O_1 in the vertical direction; the rotary reducer is located at the top of the other end of the connecting rod. Through the shaft connection, the hydraulic cylinder provides power and can rotate θ_2 around O_2 in the vertical direction. The connecting shaft is located in the middle of the rotary reducer and can rotate θ_3 around O_3 in the horizontal direction; the automatic drilling frame is placed on one

TABLE 1 $D-H$ parameters.

Rod order	Length of connecting rod a/mm	Distance between joints d/mm	Connecting rod rotation angle $a/(°)$	Joint rotation angle $\theta/(°)$	Variable range
1	0	0	90	θ_1	(0–45)
2	2054.86	0	0	θ_2	(−45–45)
3	314.48	0	90	θ_3	(0–180)
4	0	160	90	θ_4	(−90–90)
5	0	786.6	90		0

side of the connecting shaft, which can rotate θ_5, contrary to the position of the rotary reducer.

3.1 Kinematics model based on screw theory

In accordance with the principles and parameters of the $D-H$ connecting rod coordinate system of the manipulator, the homogeneous transformation relationship between the joints of the manipulator can also be expressed by the rotation matrix and the translation vector, so the homogeneous transformation moments of the front and rear joints of the manipulator are shown in Figure 3.

The homogeneous transformation matrix is expressed as T, the rotation matrix as R and translation matrix as P, then the homogeneous transformation matrix from joint $n-1$ to joint n can be expressed as ${}^{n-1}T_n$, as shown in Eq. (1). Establishment of a joint coordinate system of the manipulator by using the $D-H$ method, as shown in Figure 4.

$$ {}^{n-1}T_n = \begin{bmatrix} \cos\theta_n & -\sin\theta_n\cos\theta_n & \sin\theta_n\sin\theta_n & \alpha_n\cos\theta_n \\ \sin\theta_n & \cos\theta_n\cos\theta_n & -\cos\theta_n\cos\theta_n & \alpha_n\sin\theta_n \\ 0 & \sin\theta_n & \cos\theta_n & d_n \\ 0 & 0 & 0 & 1 \end{bmatrix} \quad (1) $$

Based on Table 1, the transformation relation matrix T_1 from coordinate system X_0-Y_0 to coordinate system X_1-Y_1 is firstly established according to the $D-H$ principle, as shown in Eq. (2). Using the same method, the subsequent transformation relation matrices between the two adjacent coordinate systems are T_2, T_3, T_4, and T_5, respectively. The expressions of the five coordinate-change matrices are shown in Eqs 3-6:

$$ T_1 = \begin{bmatrix} \cos\theta_1 & 0 & \sin\theta_1 & \alpha_1\cos\theta_1 \\ \sin\theta_1 & 0 & 0 & \alpha_1\sin\theta_1 \\ 0 & 1 & 0 & d_1 \\ 0 & 0 & 0 & 1 \end{bmatrix} \quad (2) $$

$$ T_2 = \begin{bmatrix} \cos\theta_2 & -\sin\theta_1 & 0 & \alpha_2\cos\theta_2 \\ \sin\theta_2 & \cos\theta_2 & -\cos\theta_2 & \alpha_2\sin\theta_2 \\ 0 & 0 & 1 & d_2 \\ 0 & 0 & 0 & 1 \end{bmatrix} \quad (3) $$

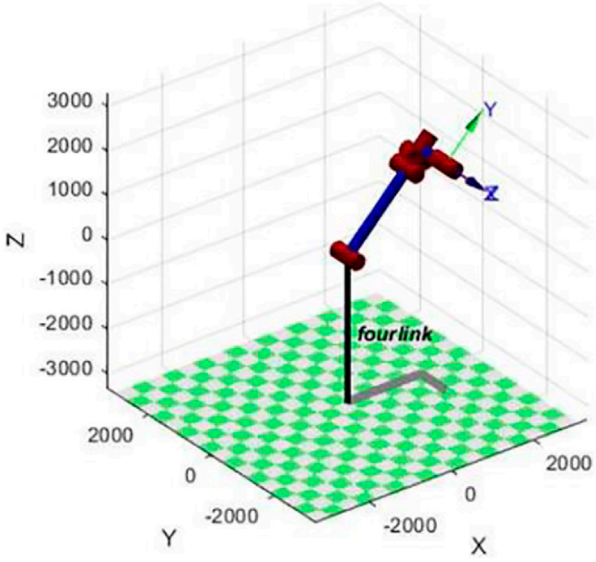

FIGURE 5
Five degrees of freedom manipulator.

$$ T_3 = \begin{bmatrix} \cos\theta_3 & 0 & \sin\theta_3 & \alpha_3\cos\theta_3 \\ \sin\theta_3 & 0 & 0 & \alpha_3\sin\theta_3 \\ 0 & 1 & 0 & d_3 \\ 0 & 0 & 0 & 1 \end{bmatrix} \quad (4) $$

$$ T_4 = \begin{bmatrix} \cos\theta_4 & 0 & \sin\theta_4 & \alpha_4\cos\theta_4 \\ \sin\theta_4 & 0 & 0 & \alpha_4\sin\theta_4 \\ 0 & 1 & 0 & d_4 \\ 0 & 0 & 0 & 1 \end{bmatrix} \quad (5) $$

$$ T_5 = \begin{bmatrix} \cos\theta_5 & 0 & \sin\theta_5 & \alpha_5\cos\theta_5 \\ \sin\theta_5 & 0 & 0 & \alpha_5\sin\theta_5 \\ 0 & 1 & 0 & d_5 \\ 0 & 0 & 0 & 1 \end{bmatrix} \quad (6) $$

All revolute joints of the manipulator in this article are represented by the $D-H$ parameters related to position and pose. The motion of the manipulator in this article is chain motion. By multiplying the homogeneous transformation matrix T_i of each joint according to the subscript number, the total

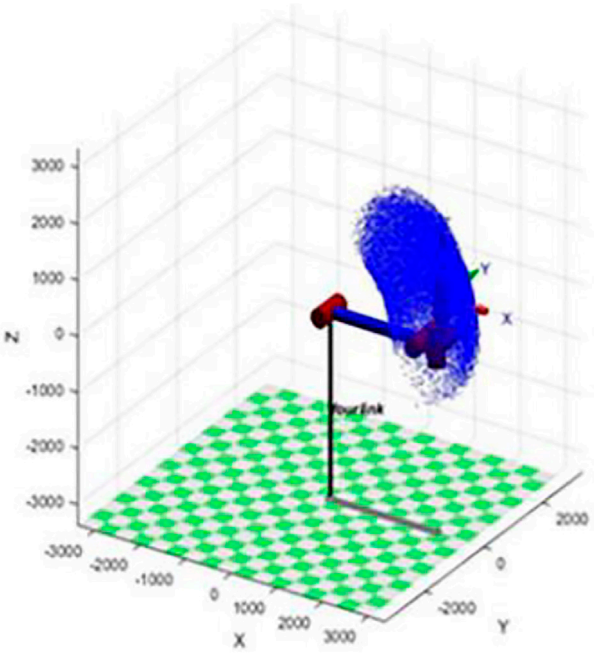

FIGURE 6
Cloud diagram of the manipulator movement space.

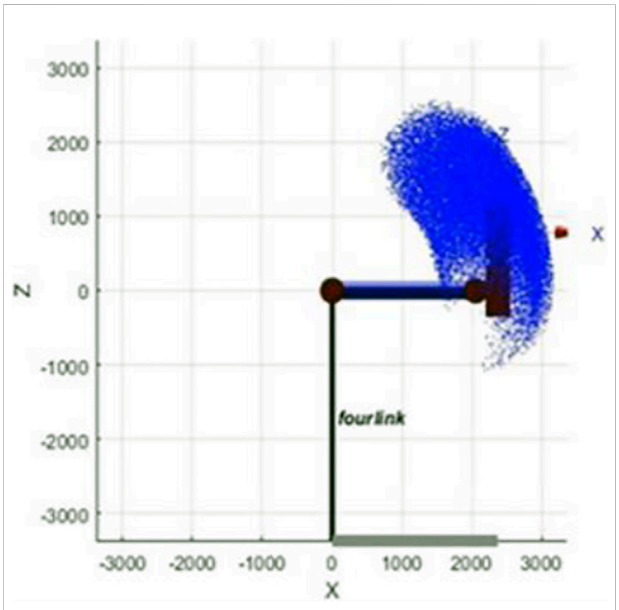

FIGURE 7
Spatial cloud diagram of the ZOX surface motion.

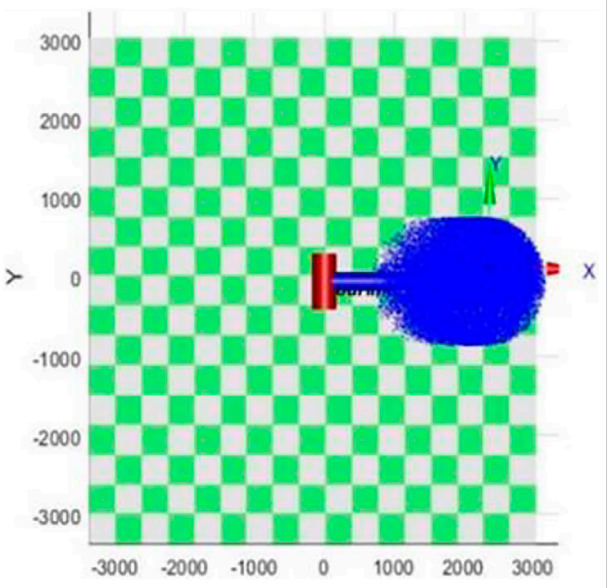

FIGURE 8
Spatial cloud diagram of the YOX surface motion.

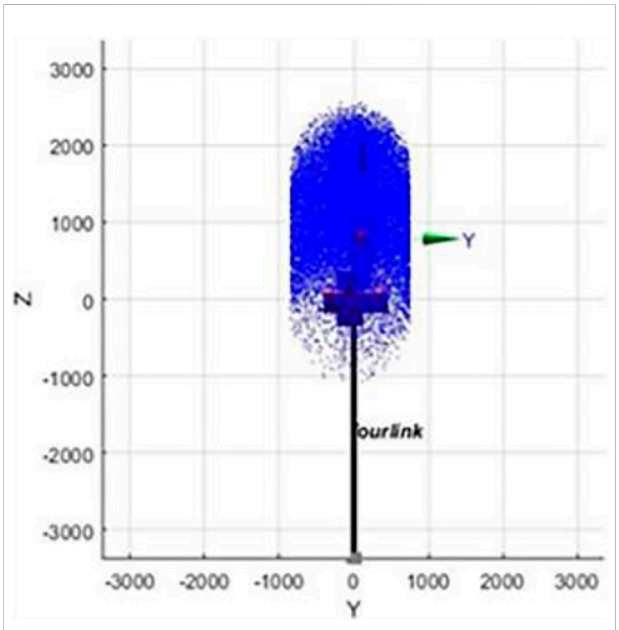

FIGURE 9
Cloud diagram of the ZOY plane motion space.

transformation matrix of the manipulator from the cloud platform to the end effector can be obtained, as shown in Eq. (7).

$$^{1}T_5 = T_1T_2T_3T_4T_5 \tag{7}$$

3.2 Motion space analysis of the manipulator

The simplified model of the manipulator of the mining roof bolter is shown in Figure 5. When the angle θ of each joint is

known, the end position X, Y, Z can be obtained; on the contrary, when the end position X, Y, Z is known, the angle of each joint can be obtained, so the inverse solution of the manipulator of the mining roof bolter can be obtained.

To describe the working space of the manipulator of the mining roof bolter, the root of the manipulator is set as $(0, 0, 0)$, and according to the forward kinematics solution of the manipulator, (x, y, z) can be obtained. The random number is obtained by using the *Rand* function in *MATLAB* in accordance with the limit of each joint, and the random value is put into the forward kinematics equation to obtain the vector of the corresponding position. The working cloud diagram of the manipulator of the mining roof bolter is obtained, as shown in Figures 6–9.

From Figures 7–9, it can be seen that the working range of the manipulator of mining roof bolter is $X \in [500, 3200]$, $Y \in [-900, +900]$, $Z \in [-1100, 2500]$; the working space of the manipulator of the mining roof bolter is approximately a part of the ellipse, and the simulated working space is compacted in the structure. Each joint of the simulated moving space is in line with the actual moving space, which can truly describe the working space of the manipulator.

4 Fractional order FOPID motion control algorithm based on WOA-FOPID parameter tuning

4.1 Fractional order control theory and the parameter tuning optimization process

4.1.1 Fractional order control theory

As a branch of the control field, fractional order control has been widely used in the design of different types of controllers (Yin et al., 2014b; Al-Saggaf et al., 2020; Sheng et al., 2021) for its advantages such as flexibility and precise parameter adjustment, increasing system stability margin and enhancing system robustness, etc. Fractional order $PI^{\lambda}D^{\mu}$ control was first proposed and demonstrated its superiority over the traditional *PID* control by Igor Podlubny through the response analysis (Podlubny, 1999; Semmari et al., 2017; Cuong et al., 2020; Dalir and Bigdeli, 2020; Bushnaq et al., 2021; Musarrat and Fekih, 2021; Nguyen et al., 2021; Wu and Huang, 2021; Huang et al., 2022). The order parameters λ, μ of the fractional order $PI^{\lambda}D^{\mu}$ controller can be taken as any real number. In the $P-I-D$ plane, values can be taken according to different controller parameters. The specific expression and range of values are shown in Figure 10.

$$C(s) = \frac{U(s)}{R(s)} = K_p + \frac{K_i}{s^{\lambda}} + K_d s^{\mu} \tag{8}$$

K_p is the proportional gain; K_i is the integral gain; $\vec{r}$ is the differential gain; $\vec{r}$ and $\vec{r}$ are the fractional, differential, and integral order, respectively.

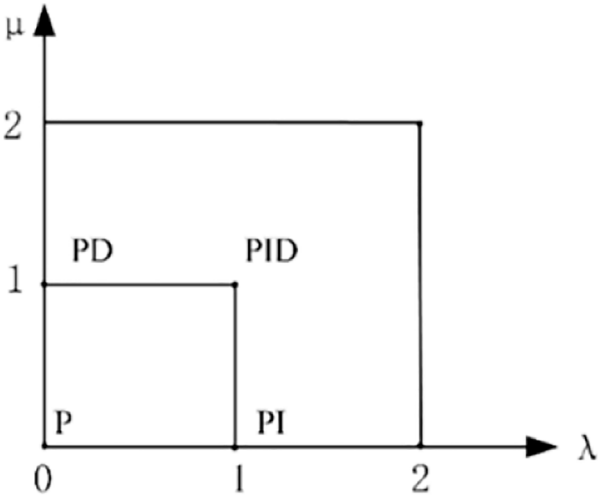

FIGURE 10
Order value range of the FOPID controller. The mathematical expression of FOPID is given.

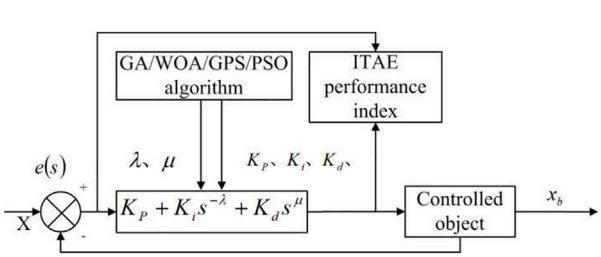

FIGURE 11
Parameter setting principle of the intelligent optimization algorithm.

Compared with the traditional *PID* control, fractional order $PI^{\lambda}D^{\mu}$ control can better subtly reflect the transition process from proportional control to integral control and differential control, so as to achieve more precision, better stability, and stronger anti-interference control effect. Therefore, the author considers designing a fractional order $PI^{\lambda}D^{\mu}$ control (FOPID) for the electronic control system of the raise boring machine in this article.

4.1.2 Parameter tuning and the optimization process

There are many kinds of parameter tuning methods. With the development of intelligent and control technology, according to the regulation characteristics of the algorithm itself, it is mainly divided into a traditional method tuning and an intelligent optimization algorithm tuning, and the latter one is widely used for its adaptability. The four intelligent optimization

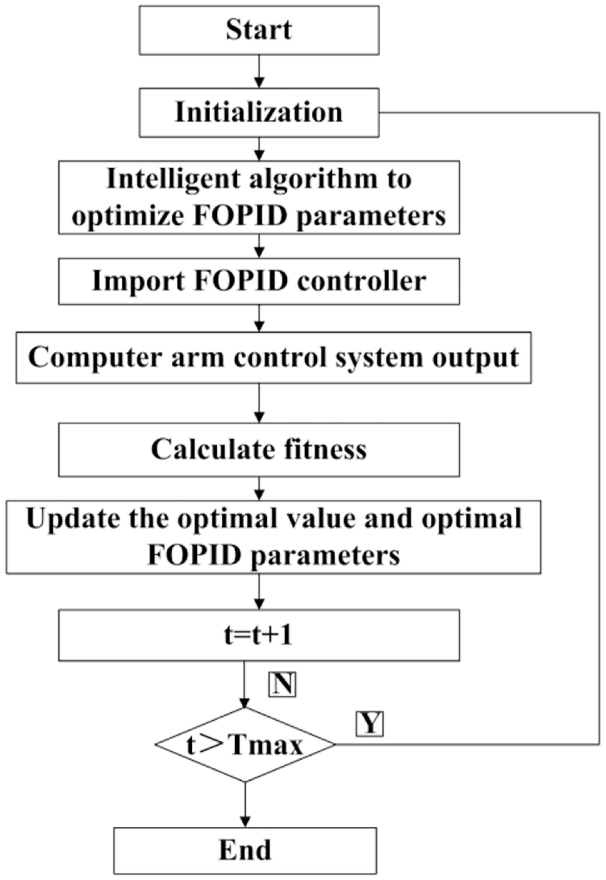

FIGURE 12
Flow chart of the intelligent optimization algorithm for tuning.

algorithms, genetic algorithm (GA), particle swarm optimization (PSO), whale algorithm (WOA), and search algorithm (GPS), have been used for real-time parameter tuning to obtain the optimal value. The parameter tuning principle of the four intelligent optimization algorithms is shown in Figure 11, and the flow chart of the intelligent optimization algorithm for tuning the FOPID parameters is shown in Figure 12. The specific mathematical theories and related expressions of the four intelligent optimization algorithms such as the whale algorithm will not be repeated.

4.2 Mathematical modeling and simulation test of the hydraulic cylinder/hydraulic motor at the joint of the manipulator

In this article, genetic algorithm (GA), particle swarm optimization algorithm (PSO), whale algorithm (WOA), and search algorithm (GPS) are combined with PID and $FOPID$, respectively, Through different combined control strategies, the control effect of the valve-controlled hydraulic cylinder is further analyzed and compared.

For the optimization algorithms used in different control strategies, an objective function is usually set to select the optimal value. The common error performance indicators include ISE (square deviation integral), ITSE (time square deviation integral), IAE (absolute deviation integral), ITAE (time absolute deviation integral), etc. In servo control, the ITAE (time absolute deviation integral) performance index weights the error, so that the error signal converges to zero as soon as possible. Therefore, this article takes the ITAE performance index as the objective function for parameter tuning (Semmari et al., 2017) as shown in Figure 11.

Here, the specific parameters of each algorithm are set as follows: PSO parameter settings: $Max\_iter = 200$, $N = 20$, $C_1 = C_2 = 1.49$; the GA parameters are set as: $N = 50$, $Max\_iter = 200$ and the variation parameter is 0.8, and the variation probability is 0.75; The $WOA - FOPID$ parameter is set to: dim = 5, $Max\_iter = 50$, $SearchAgents\_no = 100$; $WOA - PID$ is set to: dim = 3, $Max\_iter = 50$, $SearchAgents\_no = 100$, the simulation time is second (s). The comparison of different combination strategies and control indexes is shown in Tables 2, 3. Figure 11 shows the comparison of the dynamic response curves of each combination strategy of the regulating system, a is the step-response diagram of each algorithm and PID combination strategy, and b is the step-response diagram of each algorithm and $FOPID$ combination strategy. The comparison of the WOA algorithm-based PID and $FOPID$ combined control strategies is shown in Figure 11. The numerical iteration curve of the$WOA - FOPID$ fitness function is shown in Figure 11.

(1) $WE9 - 62T - HRWR160 - U - REV.D$ mathematical modeling and simulation test of the hydraulic motor

$WE9 - 62T - HRWR160 - U - REV.D$ integer order mathematical model (Dasgupta et al., 1996; Maiti et al., 2008; Long et al., 2018; Caponetto et al., 2019; Wachholz et al., 2019; Do et al., 2020):

$$G(s) = \frac{\omega_m(s)}{U(s)} = K_a \frac{K_i}{ms^2 + cs + K_s + K_y} \frac{\frac{K_q}{D_m}}{\left(\frac{s^2}{\omega_h^2} + \frac{2\xi_h}{\omega_h} + 1\right)} = \frac{1}{2.1393 \times 10^{-7}s^4 + 4.66 \times 10^{-5}s^3 + 2.79 \times 10^{-3}s^2 + 1.42 \times 10^{-2}s + 0.61} \quad (9)$$

$WE9 - 62T - HRWR160 - U - REV.D$ fractional mathematical model of the hydraulic motor (Dimeas et al., 2017; Do et al., 2020; Ma; Higazy, 2020):

TABLE 2 Mathematical modeling parameter table of the fractional integer order of the hydraulic motor.

Symbol	Parameter meaning	Parameter value	Parameter unit
K_α	Gain of proportional amplifier	0.2	A/V
ω_n	Natural frequency of valve core	15.1	——
m	Quality of valve core armature assembly	0.5	kg
ξ	Damping ratio of valve core	0.046	——
K_s	Spring stiffness	50	N/m
c	Damping coefficient of valve core armature assembly	0.7	N/m/s
K_i	Current force gain of proportional electromagnet	3	N/A
K_y	Total spring stiffness	64	N/m
K_c	Flow pressure coefficient	1.2×10^{-11}	$m^5/(N\bullet s)$
K_q	Flow gain	2.42	m2/s
K_d	Dynamic head coefficient	0.61	——
C_{tm}	Total leakage coefficient of hydraulic motor	2.65×10^{-12}	$m^5/(N\bullet s)$
D_m	Motor displacement	1.19×10^{-4}	m^3/rad
ω_d	Hydraulic natural frequency	51	Rad/s
ζ_d	Hydraulic damping ratio	0.46	——
β_e	Effective bulk modulus of elasticity	6.9×10^8	N/m^2
V_t	Total volume of hydraulic motor and connecting pipeline	3×10^{-4}	m^3
B_m	Viscous damping coefficient of hydraulic motor and load	200	$N\bullet m\bullet s/rad$
B_e	Viscous damping coefficient of reducer	3.48	$N\bullet m\bullet s/rad$
B_d	Viscous damping coefficient of power head	983.5	$N\bullet m\bullet s/rad$
J_1	Equivalent inertia of motor shaft	15	$kg\bullet m^2$
J_e	Equivalent inertia of reducer	0.476	$kg\bullet m^2$
J_d	Equivalent inertia of power head	74	$kg\bullet m^2$
C_d	Flow coefficient of solenoid proportional directional valve	0.6	——
ρ	Hydraulic oil density	860	kg/m^3
i	Transmission ratio of reducer	4.9	——

$$G(s) = \frac{\varpi_m(s)}{U(s)} = K_\alpha \frac{K_i}{ms^2 + cs + K_s + K_y} \frac{\frac{K_q}{D_m}}{\left(\frac{s^2}{\omega_h^2} + \frac{2\xi_h}{\omega_h}s + 1\right)} = \frac{1}{2.14 \times 10^{-7}s^{3.99} + 4.66 \times 10^{-5}s^{3.0042} + 0.0028s^{1.998} + 0.0143s^1 + 0.61} \tag{10}$$

Fractional order *FOPID* controller is expressed as: (Elkhazali, 2013; Maâmar and Rachid, 2014; Tolba et al., 2018):

$$G_c = 0.487 + 5.4042s^{-0.023} + 5.4837s^{1.2908} \tag{11}$$

Integer order *PID* controller expression is: (Zamani et al., 2009; Ding et al., 2017; Ren et al., 2019).

$$G_c = 30 + 1.6952s^{-2} + 24.5197s \tag{12}$$

Respectively, four types of the intelligent control algorithm are used for parameter tuning of the *FOPID* controller—integer order parameter, the *FOPID* controller—fractional order controlled object, the *PID* controller—fractional integer order controlled object, and the *FOPID* controller—fractional integer order controlled object. From Table 3 and Figure 13, according to the results of the simulation experiments, the *PID* control is not dominant in a complex system compared to FOPID, overshoot amount at about 30%, and settling time floating around 0.7 s; According to the results of the data based on *WOA* algorithm parameters tuning of the system has a certain advantage, settling time reduced to 0.3 s.

On the whole, the *FOPID* controller has shown a better control effect on the fractional order-controlled object, and the overshoot has been reduced. According to the data results, the optimization ability of the *WOA* algorithm is obvious, which makes the controlled system have better stability. For the fractional controlled object, the stability can be achieved in 0.19s, and the overshoot is 3.49%. This fully reflects the superiority of the fractional order *FOPID* controller, as shown in Figure 13.

In response speed, adjustment time, and steady-state accuracy, the fractional order *WOA – FOPID* controller has a

TABLE 3 Hydraulic motor's parameter table.

Combinations	Dynamic indicators		
	Standard deviation	Overshoot (%)	Settling time/s
GA – FOPID -Integer order	0.05865	39	0.29
PSO – FOPID -Integer order	0.05853	38.72	0.28
GPS – FOPID -Integer order	0.0444	23.45	0.41
Optimal-*FOPID* -Integer order	0.05869	38.819	0.28
WOA – FOPID -Integer order	0.03653	15.18	0.09
GA – FOPID -Fractional order	0.03944	27.91	0.59
PSO – FOPID -Fractional order	0.0475	25.52	0.52
GPS – FOPID -Fractional order	0.04547	26.12	0.39
Optimal-*FOPID* -Fractional order	0.05803	37.67	0.28
WOA – FOPID -FrActional order	0.05529	3.49	0.19
GA – PID -Integer order	0.04421	29.59	0.7
PSO – PID -Integer order	0.04421	29.6	0.7
GPS – PID -Integer order	0.04421	29.6	0.7
Optimal-*PID* -Integer order	0.07034	53.57	0.27
WOA – PID -Integer order	0.04092	27.03	0.34
GA – PID -Fractional order	0.0448	30.7	0.67
PSO – PID -Fractional order	0.0448	30.7	0.67
GPS – PID -Fractional order	0.0448	30.7	0.67
Optimal-*PID* -Fractional order	0.07027	53.3	0.27
WOA – PID -Fractional order	0.4019	26.27	0.31

better control effect than the fractional order *GPS – FOPID* controller, integer order *GPS – PID* controller, fractional order *GA – FOPID* controller, integer order *GA – PID* controller, fractional order *PSO – FOPID* controller, integer order *PSO – PID* controller, and integer order *WOA – FD* controller. In this study, the intelligent optimized whale algorithm *WOA* is directly applied to the systematic controllers of the oil cylinder *DOA*090470 – 1 (1) and *DOA*090260 – 1 in the manipulator for parameter tuning, and the control strategies of different combinations are compared and analyzed (Table 4).

(2) Mathematical modeling and simulation test of the hydraulic cylinder *DOA*090470 – 1 (1)

The integer order mathematical model of the hydraulic cylinder *DOA*090470 – 1 (1) (Zhan et al., 2015; Dingyu, 2020):

$$G(s) = \frac{X_P}{U} = \frac{\frac{K_q}{A_p}K_i k_x}{s\left(\frac{s^2}{\omega_h^2} + \frac{2\xi_h}{\omega_h}s + 1\right)} = \frac{48.625}{s\left(3.6 \times 10^{-3}s^2 + 0.727s + 1\right)} \tag{13}$$

$$G(s) = \frac{X_P}{U} = \frac{\frac{K_q}{A_p}K_i k_x}{s\left(\frac{s^2}{\omega_h^2} + \frac{2\xi_h}{\omega_h}s + 1\right)} = \frac{48.625}{s\left(7.38 \times 10^{-4}s^{2.0214} + 1.48 \times 10^{-3}s^{0.9731} + 1.99 \times 10^{-2}\right)} \tag{14}$$

Integer order *PID* controller expression (Elkhazali, 2013; Maâmar and Rachid, 2014; Tolba et al., 2018):

$$G_c = 18.4022 + 30s^{-1} \tag{15}$$

Fractional order *FOPID* controller expression (Zamani et al., 2009; Ding et al., 2017; Ren et al., 2019):

$$G_c = 29.9442 + 29.9660s^{-0.0308} + 13.1634s^{1.104} \tag{16}$$

Figure 14 and Table 5 show that the *PID* controller is not fit in complex systems, and the results show that it fails to fulfill fine-tuning, especially as the controlled object gradually stabilizes after 6.06s when the *PID* fractional order acts. In the complex system, the *FOPID* controller has a better control effect on the fractional order controlled object, and the overshoot is 8.672%, which can be settled in 0.02s. The*DOA*090470 – 1 (1) hydraulic cylinder parameter is shown in Table 6.

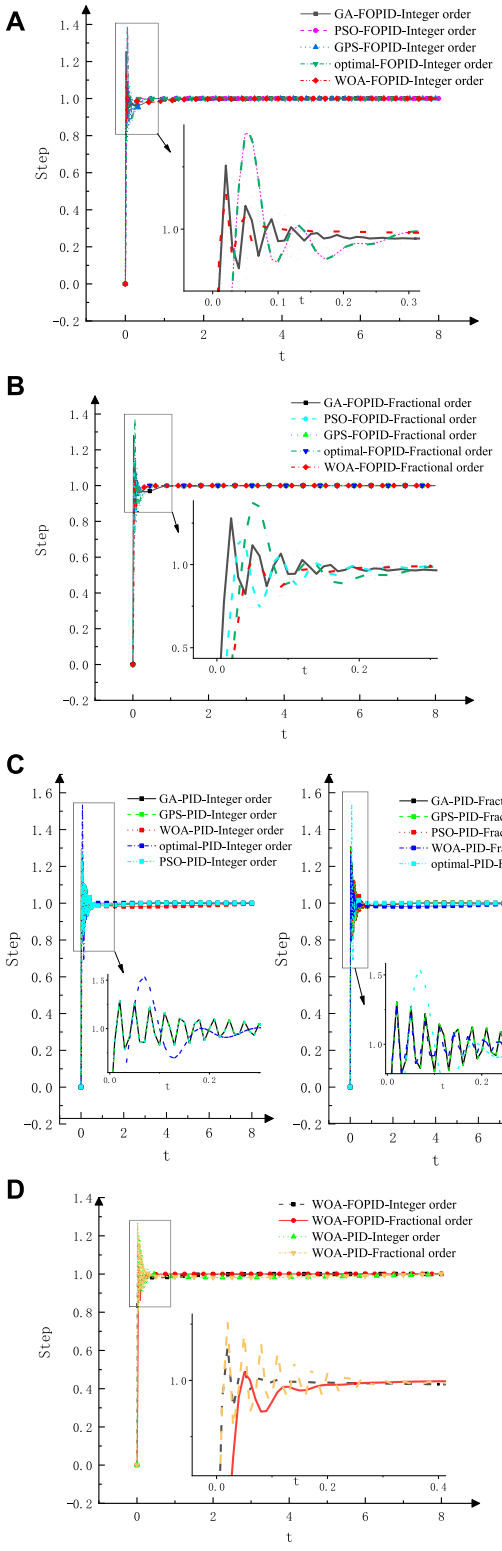

FIGURE 13
Control effect and step response of different combination strategies of the hydraulic motor. **(A)** The intelligent control

(*Continued*)

FIGURE 13 | algorithm for FOPID controller - integer order parameter setting diagram of controlled objects; **(B)** Parameter tuning diagram of FOPID controller-fractional controlled object by intelligent control algorithm; **(C)** Intelligent control algorithm PID controller - fractional integer order controlled object parameter setting diagram; **(D)** The intelligent control algorithm for FOPID controller - fractional integer order parameter setting graph of controlled objects.

(3) Mathematical modeling and simulation test of the hydraulic cylinder *DOA*090260 − 1

Integer order mathematical model of the hydraulic cylinder *DOA*090260 − 1 (Zhan et al., 2015; Dingyu, 2020):

$$G(s) = \frac{X_P}{U} = \frac{\frac{K_q}{A_p}K_i k_x}{s\left(\frac{s^2}{\omega_h^2} + \frac{2\xi_h}{\omega_h}s + 1\right)} = \frac{48.625}{s\left(2 \times 10^{-3}s^2 + 0.0726s + 1\right)} \tag{17}$$

$$G(s) = \frac{X_P}{U} = \frac{\frac{K_q}{A_p}K_i k_x}{s\left(\frac{s^2}{\omega_h^2} + \frac{2\xi_h}{\omega_h}s + 1\right)} = \frac{48.625}{s\left(4.11 \times 10^{-5}s^{1.9946} + 0.0015s^{0.9989} + 0.02\right)} \tag{18}$$

Expression of the integer order PID controller [41–43]:

$$G_c = 11.2292 + 30s^{-2} + 1.35 \times 10^{-8}s \tag{19}$$

Expression of the fractional order *FOPID* controller (Zamani et al., 2009; Ding et al., 2017; Ren et al., 2019):

$$G_c = 0.4758 + 27.2283s^{-2.5323} + 29.9673s^{1.0212} \tag{20}$$

Figure 15 and Table 7 show that the *FOPID* controller has a better control effect for fractional controlled objects, and the overshoot can reach 6.84% in 0.5s. On the whole, the *FOPID* controller is more stable than the *PID* controller, and the *PID* control strategy shows almost the same control effect, which is about 20%. In the actual support work of the manipulator, if there is an overshoot in the oil cylinder displacement control system, it will lead to the inaccurate positioning in the drilling hole, which will take more time, and even influence the effectiveness of electronic components in the manipulator. If 16 bolts need to be installed in a roadway section, the mechanical arm takes one more minute for installation of each bolt due to the overshoot, and takes another 16 min in total to complete the support work of a section. Cost function vs. iterations is plotted for the mathematical modeling and simulation tests of the hydraulic cylinder, as shown in Figure 16.

TABLE 4 Doa090470-1 (1) hydraulic cylinder parameter table.

No.	Symbol	Parameter meaning	Parameter value	Parameter units
1	X_p	Piston displacement of hydraulic cylinder	--	--
2	ω_h	Hydraulic natural frequency	16.77	*rad/s*
3	M	Total load quality	--	*Kg*
4	ξ_h	Hydraulic damping ratio	0.61	--
5	B_p	Viscous damping coefficient of load	--	--
6	k_x	Gain of Electro - hydraulic Proportional Valve	7.78×10^{-4}	--
7	K_i	Gain of proportional amplifier	0.2	---
8	K_q	Flow Gain of Hydraulic Cylinder	300	--
9	U	Potential signal	--	--
10	A_p	Effective area of piston	9.6×10^{-4}	m^3

Fractional order mathematical model of hydraulic cylinder *DOA*090470 – 1(1).

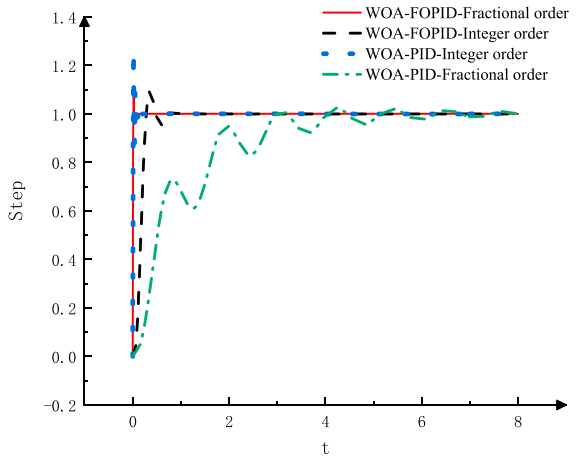

FIGURE 14
*DOA*090470 – 1(1) step response diagram of the control effect of different combination strategies of the hydraulic cylinder.

5 Experiment

In order to verify the correctness and effectiveness of the control strategy in the manipulator control system of the mining roof bolter, the ground training and industrial tests were carried out in the underground roadway, as shown in Figure 17 and Figure 18. The test platform is the underground roadway, with a section height of 2.8–4 m, a width of 3.8–5.6 m, a maximum inclination of 20°, and a maximum drilling depth of 8.3 m. All of them are in a gas-free working environment. The test lasted a total of 9 days. In the first test, there were 14 anchor cable holes of 8.3 m, with a total of 116 m; 46.3 m anchor cable holes, 25 m in total; 124 m anchor cable holes, 48 m in total. In the second test, there were 6 anchor cable holes of 4 m, with a total of 24 m; 6.3 m anchor cable holes, totaling 37 m; 122.5 m anchor cable holes, 30 m in total.

5.1 Composition of the control system

The plan of an electric–control system is shown in Figure 19. The control system adopts a modular design, and each functional module runs independently without interference, so as to avoid whole equipment paralysis due to a single failure. The electric control system can be divided into five modules: main circuit unit, power unit, protection unit, signal conditioning isolation unit, and logic control unit. The block diagram of the control system module is shown in Figure 20.

TABLE 5 Comparison of different combination strategies and control indexes of the *DOA*090470 – 1(1) hydraulic cylinder.

Combination	Dynamic indicators		
	Standard deviation	Overshoot (%)	Settling time/s
WOA – FOPID -Integer order	0.1307	9.5	0.68
WOA – FOPID -Fractional order	0.03571	8.672	0.02
WOA – PID -Integer order	0.03753	25.78	0.09s
WOA – PID -Fractional order	0.2206	2.5	6.06s

TABLE 6 *DOA*090470 – 1(1) hydraulic cylinder parameter table.

No	Symbol	Parameter meaning	Parameter value	Parameter units
1	ω_h	Hydraulic natural frequency	22.6	
2	ς_h	Hydraulic damping ratio	0.82	
3	A_p	Effective area of piston	9.6×10^{-4}	m^3
4	V_t		2.5×10^{-4}	
5	K_x	Gain of electro-hydraulic proportional valve	300	
6	K_q	Flow Gain of Hydraulic Cylinder	7.78	
7	K_i	Gain of proportional amplifier	0.2	
8	M	Total load quality	2×10^4	kg

Fractional order mathematical model of hydraulic cylinder *DOA*090260 – 1 .

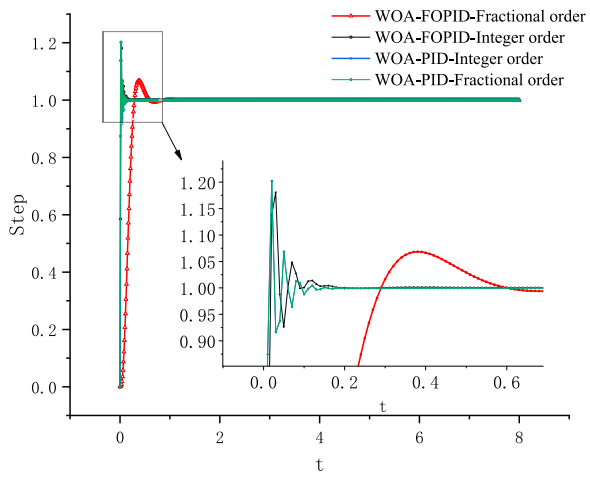

FIGURE 15
WOA-FOPID–fractional transfer function unit step diagram.

The main circuit module defines the main structure of the system, and the isolation switch is applied as the switch of the main circuit power supply of the electrical control box to control the oil pump circuit. In terms of control, a vacuum contactor is used in the oil pump circuit, and installed the resistance and capacitance absorption device, to absorb the high voltage generated by the motor in the vacuum contactor disconnection. There are three current transmitters on the cables of each circuit to complete the acquisition of analog quantity.

The power module is mainly composed of a main transformer and four air circuit breakers. The main transformer has three voltage ranges of the input tap: 1,250, 1,140, and 1,025 V. When the voltage is unstable in the coal mine, the transformer tap can be adjusted with the voltage change to ensure the stability of the output voltage, and then ensure the reliability of the control loop. A 24 V tap provides power for the lamp, 220 V for the contactor coil and power modules, and 127 V for the intrinsic safe power supply.

The short-circuit protection of the main circuit and the transformer circuit is realized by a circuit breaker. The motor over-current, overload, and phase break of each driving mechanism are prevented by the *PLC* controller. Leakage locking, leakage monitoring, and overheating are prevented by using an integrated protector. Signal acquisition of the main circuit and the control circuit by a current transmitter and protection unit on each branch cable is processed and judged by an electronic circuit and controller program.

The signal isolation module and the signal conversion module together constitute the signal conditioning isolation module. The isolation module realizes the conversion of (non) intrinsic safety signal, the input and output of various controllers and peripheral devices in the control system. The logic control

TABLE 7 Comparison of different combination strategies and control indicators.

Combination	Dynamic indicators		
	Standard deviation	Overshoot (%)	Settling time/s
WOA – FOPID-Integer order	0.03923	18.04	0.09
WOA – FOPID-Fractional order	0.1247	6.84	0.5
WOA – PID-Integer order	0.03663	20.3	0.09
WOA – PID- Fractional order	0.0366	20.12	0.09

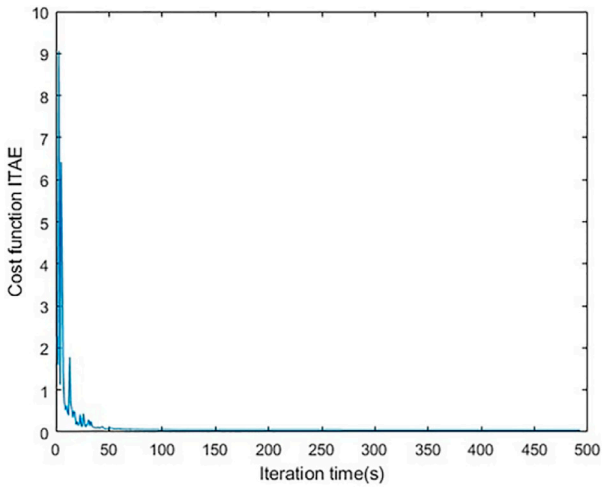

FIGURE 16
Cost function vs. iterations.

FIGURE 17
Ground experiment.

unit is the core part of the entire electrical system, which can complete various protection functions and communication functions of the motor, and also realize the corresponding

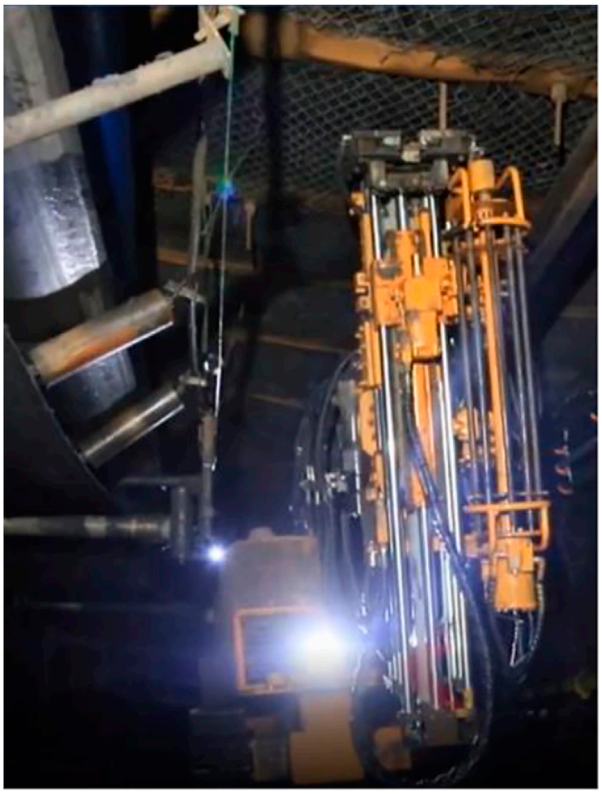

FIGURE 18
Downhole experiment.

control functions: the actual running state of each motor is judged through the calculation and processing of the collection parameters of the system; if a fault occurs, appropriate trip instructions are issued according to the type of fault.

5.2 Hardware structural design of the control system

The control cabinet consists of a PLC controller module, HMI module, and a receiver module. Each working condition monitoring unit and input/output driving unit cooperate with each other to ensure the stable operation of each control function of the system. The hardware structure block diagram of the control system is shown in Figure 19. Digital input drive unit, analog input drive unit, and the antenna are the control center of the main input module, in which the knob and switch sensor units input information to the digital input drive unit; the handle potentiometer and analog sensor input information to the analog input drive unit; the remote transmitter inputs information to the receiver module through the antenna. The digital output drive unit comprises of a light, an indicator light, and a switching electro-magnetic valve; the analog output drive unit

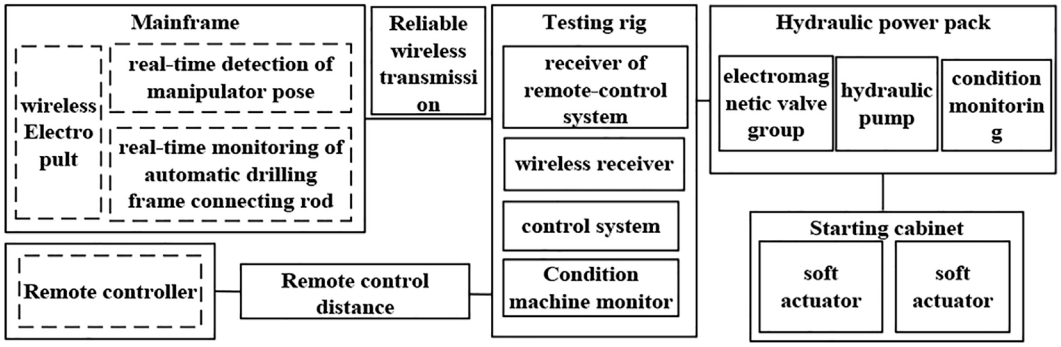

FIGURE 19
General scheme of an electric control system for the mining roof bolter.

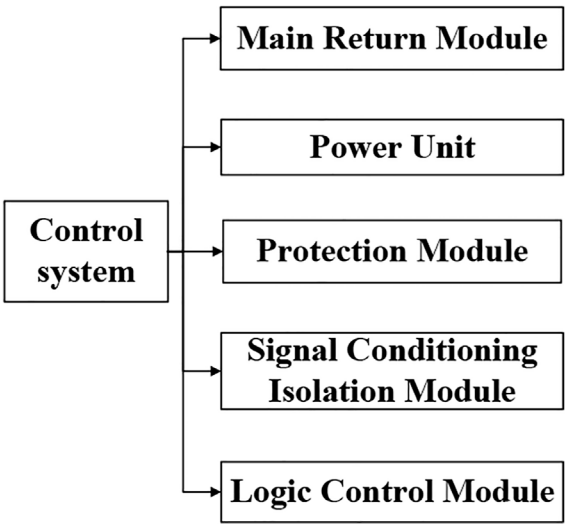

FIGURE 20
Composition of a control system module.

includes a variable pump and a proportional electro-magnetic valve. The hardware structural block diagram is shown in Figure 21. In addition, this study carried out the design of the power circuit and selection of the main components.

5.3 Control system software composition

The software system is composed of an operation signal processor, video signal processor, fault information alarm software, equipment parameter setting software, data display and analysis software, data storage and analysis software, and signal output control software. Its structural block diagram is shown in Figure 22.

5.4 Control principle

The electronic control system adopts the Siemens 200 series *PLC* host and its corresponding expansion module (analog output/input), and communicates with the remote control receiving unit through the *PLC* host's own *RS*485 communication interface (*Modbus* · *RTU*) , so as to precisely conduct motions, such as pump motor start and stop, large manipulator movements, expansion of the front and rear top tightening cylinders, forward and reverse rotations of the rotary motor, cylinder's forward and backward, horizontal rotary positively and negatively, vertical rotary positively and negatively, adjustment of the oil cylinder, cylinder of gripper opening and closing, upper rod of manipulator sending, opening and closing of manipulator, drilling rod storeroom forward and reversing rotary, pin hydraulic cylinder opening and closing, water valve opening and closing, detection and protection of the hydraulic system through the acquisition of oil tank temperature and hydraulic system pressure sensor signals, and the display on the remote transmitter screen through *RS*485 communication. A position sensor is installed to detect the position of the mainframe and the drilling rod store to ensure the precision control of automatic drilling/un-drilling. Motor intelligent integrated protector can display the real-time voltage and current of the system, with protection functions avoiding over voltage, under voltage, overload, short circuit, circuit break, phase break, leakage, display, and store alarm fault in real time. A proportional electro-hydraulic valve can adjust the hydraulic valve opening and pressure value through the *PWM* output signal of the *PLC* analog expansion module and proportional amplifier. Manual/automatic control of a locomotive can be realized by an internal ladder diagram program operation. Automatic control adopts the one-button operation, where the equipment can automatically complete the drilling/un-drilling process and have the suspension function and the one-button emergency stop function for the operator to deal with the emergency situation in the process of an automatic operation.

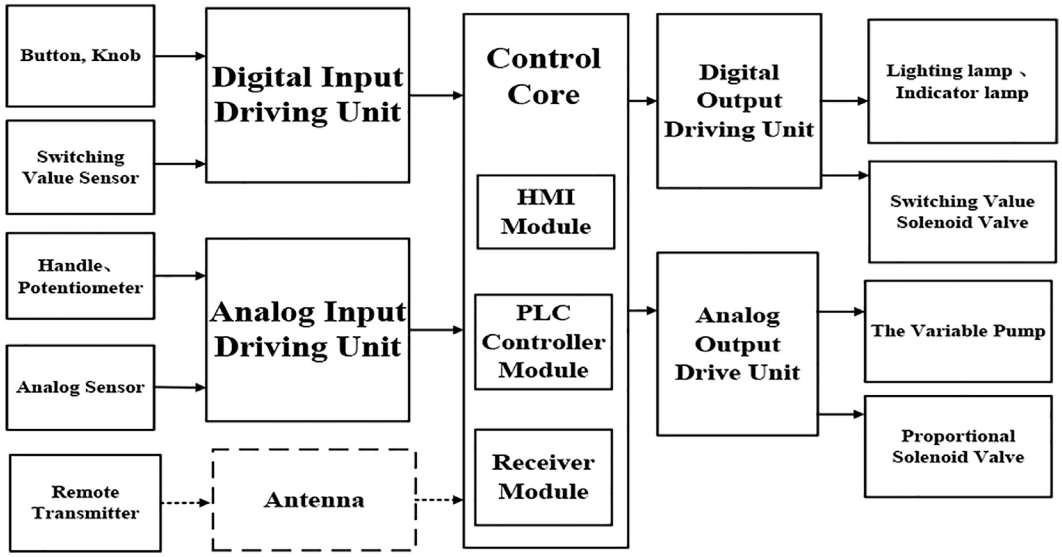

FIGURE 21
Hardware structure block diagram of the control system.

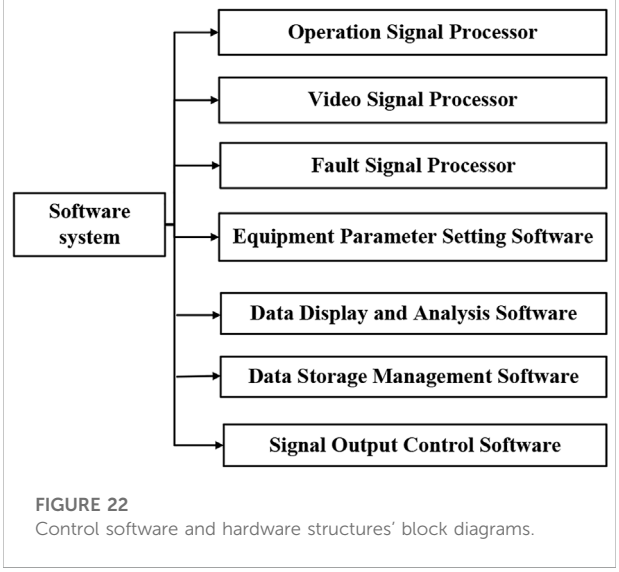

FIGURE 22
Control software and hardware structures' block diagrams.

5.5 Implementation plan

A hydraulic anchor rod drill truck was carried out to the ground training drill from August 22 to August 23,2019, arrived to the coal mine on August 24, on August 25, in 11,505W, the transport lane carried out an industrial test, on August 26 implemented fire debugging, operation, and on August 28 began an advanced supporting anchor cable test behind the excavator. The periodic summary is as follows:

As of September 9, 38 holes were drilled, among which 35 were anchored, 3 holes were drilled during the test, respectively 3.0, 5.0, and 5.5 m, without anchoring.

With a 6.3 m grouting anchor, it takes about 4 min on average to move forward to adjust the position of the drill truck, 14 min on average to drill, 8 min on average to withdraw the drill, 4 min on average to install the anchor cable, and 30 min on average in total. Fourteen representative boreholes in the early experimental period were selected for analysis, as follows in Table 8.

According to the experimental conclusions:

(1) After the control system design is completed, it is debugged and applied on the roof bolter. The control system realizes the remote pump station start–stop control, hydraulic cylinder position control, and meets the requirements of the process operation. The experiment proves that the $WOA-FOPID$ control strategy in an electro-hydraulic drive control system of effectiveness. The control strategy can make the electric hydraulic drive control in good real-time performance, accuracy, and rapidity. The manipulator can achieve high precision control in the underground roadway and can be used as a new control method for roof bolter.
(2) The automatic support system of the manipulator of the mining roof bolter breaks through the technology of automatic transportation of anchoring agents and the technology of transportation bolts and cables, and realizes a real automatic support working line without man-made

TABLE 8 Test record of the anchor rod drill truck.

Times	Drilling time	Undrilling time	Anchor installation	Truck moving	Total minutes
1	10:25–10:42	10:42–10:55	10:55–11:01	11:01–11:06	41
2	9:35–10:05	10:05–9:43	9:43–9:48	9:48–9:52	37
3	9:15–9:31	9:31–9:43	9:43–9:48	9:48–9:52	37
4	12:22–12:39	12:39–12:49	12:51–12:56	12:58–13:04	38
5	9:32–9:46	9:46–9:54	9:54–9:58	9:59–10:03	30
6	10:31–10:48	10:48–11:03	11:03–11:06	11:07–11:50	39
7	11:18–11:31	11:31–11:39	11:39–11:43	11:44–11:50	31
8	11:57–12:10	12:10–12:18	12:18–12:23	12:23–12:28	31
9	12:47–13:00	13:00–13:14	13:17–13:20	13:20–13:24	34
10	13:44–1:59	13:50–14:08	14:08–14:12	Stop	28
11	10:50–11:08	11:08–11:15	13:34–13:38	11:18–11:20	30
12	11:21–12:56	12:56–13:05	13:05–13:09	12:38–12:42	81
13	12:42–12:56	12:56–13:05	13:05–13:09	13:15–13:20	32
14	13:25–13:40	13:40–13:52	13:52–13:54	Stop	29

interference. The manipulator can automatically drill bolt holes, cable holes, cut top holes, coal powder detection holes, water injection holes, and 360° all-round drilling. In the later stage, the automatic support working line can be combined with the automatic tunneling cutting, and the unmanned driving face can be built.

6 Conclusion

To find whether the mining roof bolter can realize precise hole positioning, in a complex environment, this article uses *FOPID* control fine-tuning features in a non-linear control object, proposes a method based on the whale algorithm (*WOA*) for *FOPID* parameter tuning. Through establishing the electro-hydraulic coupling model of the hydraulic motor and hydraulic cylinder at four joints of the manipulator of the mining roof bolter and the simulation analysis in *Matlab/Simulink* , the following conclusions can be obtained:

(1) From the model built from *Matlab/Simulink* and the objective function *WOA* numerical iteration process, it can be found that the *WOA* has good optimization ability and convergence performance, which verifies the excellent performance of *WOA* in the control parameter tuning. The *WOA – FOPID* control strategy has a certain anti-interference performance, and can be timely corrected when the electro-hydraulic coupling model of the manipulator is disturbed, so that all parameters can fluctuate in a small range, which has a good engineering application prospect.

(2) The effectiveness of the *WOA – FOPID* control strategy in the electro-hydraulic drive control system can be verified by the industrial test on the mining roof bolter. The control strategy can make the electro-hydraulic drive control in good real-time performance, accuracy, and rapidity.

Data availability statement

The original contributions presented in the study are included in the article/supplementary material; further inquiries can be directed to the corresponding author.

Author contributions

Writing the original draft, ZJ; Funding acquisition, ZJ; Data curation, WY, CL, WN, BY, and WC. All authors have read and agreed to the published version of the manuscript.

Funding

The author wishes to thank the Youth fund of National Natural Science Foundation of China (No. 52104165), Free exploration general fund of Shanxi Provincial Department of science and technology (No: 20210302123123), State Key Laboratory of robotics and systems (No.SKLRS-2021-KF-16).

Conflict of interest

ZJ was employed by China Coal Science and Industry Group Co., Ltd. and Ningxia Tiandi Benniu Industrial Group Co., Ltd. CL, WN, and BY were employed by China Coal Science and Industry Group Co., Ltd. The remaining authors declare that the research was conducted in the absence of any commercial or financial relationships that could be construed as a potential conflict of interest.

Publisher's note

All claims expressed in this article are solely those of the authors and do not necessarily represent those of their affiliated organizations, or those of the publisher, the editors, and the reviewers. Any product that may be evaluated in this article, or claim that may be made by its manufacturer, is not guaranteed or endorsed by the publisher.

References

Al-Saggaf, U., Mansouri, R., Bettayeb, M., Mehedi, I. M., and Munawar, K. (2020). Robustness improvement of the fractional order LADRC scheme for integer high order system, IEEE Transactions on Industrial Electronics (ISSN:0278-0046), 99. IEEE, 1. doi:10.1109/TIE.2020.3016258

Author Anonymous State Administration of coal mine safety Key R & D catalogue of coal mine robot [Z] Announcement No. 1, 2019.

Bushnaq, S., Saeed, T., Torres, D. F. M., and Zeb, A. (2021). Control of COVID-19 dynamics through a fractional-order model. *Alexandria Eng. J.*, 3587–4359. (ISSN.1110-0168). doi:10.1016/j.aej.2021.02.022

Caponetto, R., Machado, J. T., Murgano, E., and Xibilia, M. G. (2019). Model order reduction: A comparison between integer and non-integer order systems approaches. *Entropy* 9, 876. (ISSN:1099-4300) 21. doi:10.3390/e21090876

Chen, Wei, Yu, Y, and Zhao, X (2013). Position control strategy and experimental research of 2R underactuated planar flexible manipulators. *J. Mech. Eng.* 49 (23), 80. (ISSN:1823-5514). doi:10.3901/jme.2013.23.080

Cuong, H. M., Quoc Dong, H., Trieu, P. V., and Tuan, L. A. (2020). Adaptive fractional-order terminal sliding mode control of rubber-tired gantry cranes with uncertainties and unknown disturbances. *Mech. Syst. Signal Process.* 154, 107601. (ISSN:0888-3270). doi:10.1016/j.ymssp.2020.107601

Dalir, M., and Bigdeli, N. (2020). The design of a new hybrid controller for fractional-order uncertain chaotic systems with unknown time-varying delays. *Appl. Soft Comput.* 87, 106000. doi:10.1016/j.asoc.2019.106000

Dasgupta, K., Mukherjee, A., and Maiti, R. (1996). Modeling and dynamics of epitrochoid generated orbital rotary piston lsht hydraulic motor: A bondgraph approach. *J. Manuf. Sci. Eng.* 118, 415–421. doi:10.1115/1.2831046

Dimeas, I., Petras, I., and Psychalinos, C. (2017). New analog implementation technique for fractional-order controller: A dc motor control. *AEU - Int. J. Electron. Commun.* 78, 192–200. doi:10.1016/j.aeue.2017.03.010

Ding, Y., Xu, J., Cao, J., and Zhang, D. (2017). Mathematical modeling about nonlinear delayed hydraulic cylinder system and its analysis on dynamical behaviors. *Discrete Cont. Dyn. S* 10 (5), 943–958. doi:10.3934/dcdss.2017049

Dingyu, P. X. (2020). *Lecture hall Volume 4 MATLAB optimization calculation [M*. Beijing: Tsinghua University Press.

Do, T. C., Trần, T. D., Dinh, T. Q., Ahn, K. K., et al. (2020). Tracking control for an electro-hydraulic rotary actuator using fractional order fuzzy PID controller. *Electronics*, 926. (ISSN:2079-9292) 9.6. doi:10.3390/electronics9060926

Elkhazali, R. (2013). *Fractional-order PI λD controller design[M]*. Pergamon Press.

Feng, G.-L., Chen, B.-R., Xiao, Y.-X., Jiang, Q., Li, P.-X., Zheng, H., et al. (2022). Microseismic characteristics of rockburst development in deep tbm tunnels with alternating soft-hard strata and application to rockburst warning: A case study of the neelum-jhelum hydropower project. *Tunn. Undergr. Space Technol.* 122, 104398. doi:10.1016/j.tust.2022.104398

Feng, G.-L., Feng, X.-T., Chen, B.-r., Xiao, Y.-X., and Yu, Y. (2015). A microseismic method for dynamic warning of rockburst development processes in tunnels. *Rock Mech. Rock Eng.* 48 (5), 2061–2076. doi:10.1007/s00603-014-0689-3

Ge, S., and Hu, P. W (2020). Coal mine robot system and key technology. *J. coal* 45 (01), 455–463. (ISSN: 0166-5162).

Higazy, M. (2020). Novel fractional order SIDARTHE mathematical model of COVID-19 pandemic. *Chaos, Solit. Fractals* 138, 110007. ISSN:0960-0779. doi:10.1016/j.chaos.2020.110007

Huang, S., Wang, J., Huang, C., Zhou, L., Xiong, L., Liu, J., et al. (2022). A fixed-time fractional-order sliding mode control strategy for power quality enhancement of PMSG wind turbine. *Int. J. Electr. Power & Energy Syst.* 134, 107354. (ISSN:0142-0615). doi:10.1016/j.ijepes.2021.107354

Jing, X, and pan, X. W (2018). Fuzzy PID *attitude* control of pesticide spraying four axis aircraft. *J. drainage irrigation Mech. Eng.* 36 (5), 7. doi:10.3969/j.issn.1674.8530.17.0187

Kang, H. P. (2007). *Wang Jinhua Roadway bolt support theory and complete set of technology [M]*. Beijing: Coal Industry Press.

Li, F., Hu, J., and Zhang, D. R. (2019). Development and application status and trend of coal mine robot. *China coal.*. 045 (007), 28–32. doi:10.19880/j.cnki.ccm.2019.07.005

Li, R., Cao, J., Xue, C., and Manivannan, R. (2021). Quasi-stability and quasi-synchronization control of quaternion-valued fractional-order discrete-time memristive neural networks. *Appl. Math. Comput.* 395, 125851. (ISSN:0096-3003). doi:10.1016/j.amc.2020.125851

Li, Z, and Xing, l (2007). Submarine robot automatic tracking scheduled mining path control. *J. Mech. Eng.* 43 (1), 6. doi:10.3321/j.issn:0577-6686.2007.01.025

Liu, F., Cao, W., and Zhang, J. (2021). Scientific and technological innovation progress of China's coal industry and the development direction of the 14th five year plan. *J. coal* 46 (1), 1–15. doi:10.13225/j.cnki.jccs.2021.0042

Long, Z-M., Guan, B-J., Chen, S-Y., Chen, G-J., and Guo, S-Q. (2018). "Modeling and simulation of hydraulic motor tracking servo motor driving load," in ICSGEA, 118–121. doi:10.1109/icsgea.2018.00037

Luo, Y, Du, L, Zhou, S, and Luo, K (2021). Simulation *research* on electro-hydraulic proportional position control system of blanking based on fuzzy PID. *Mach. tool hydraulic*. doi:10.3969/j.issn.1001-3881.2021.22.030

Ma, F. *Research on Modeling and control of single-phase PWM rectifier based on fractional order*. Zhengzhou: Henan University of technology.

Maâmar, B., and Rachid, M. (2014). IMC-PID-fractional-order-filter controllers design for integer order systems. *ISA Trans.* 53, 1620–1628. 0019-0578*)* 53. doi:10.1016/j.isatra.2014.05.007

Maiti, D., Biswas, S., and Konar, A. (2008). Design of a fractional order PID controller using particle swarm optimization technique. *Int. J. Adv. Manuf. Technol.*, 521–531. *ISSN:0268-3768)* 58.5-8.

Musarrat, M. N., and Fekih, A. (2021). A fractional order sliding mode control-based topology to improve the transient stability of wind energy systems. *Int. J. Electr. Power & Energy Syst.* 133, 107306. (ISSN:0142-0615). doi:10.1016/j.ijepes.2021.107306

Nguyen, D., Bao, D. L., and Choi, S-B. (2021). Smart dampers-based vibration control–Part 2: Fractional-order sliding control for vehicle suspension system. *Mech. Syst. Signal Process.* 148, 107145. (ISSN:0888-3270). doi:10.1016/j.ymssp.2020.107145

Podlubny, I. (1999). Fractional-order systems and PI/sup/spl lambda//D/sup/spl mu//-controllers. *IEEE Trans. Autom. Contr.* 44, 208–214. doi:10.1109/9.739144

Ren, H. P., Fan, J. T., and Kaynak, O. (2019). "Optimal design of a fractional-order proportional-integer-differential controller for a pneumatic position servo system," in IEEE Transactions on Industrial Electronics (IEEE). (ISSN:0278-0046). doi:10.1109/TIE.2018.2870412

Semmari, H., Mauran, S., and Stitou, D. (2017). Experimental validation of an analytical model of hydraulic motor operating under variable electrical loads and pressure heads. *Appl. Energy* 206, 1309–1320. (ISSN:0306-2619). doi:10.1016/j.apenergy.2017.10.010

Sheng, Y., Bai, W., and Xie, Y. (2021). Fractional-order $$PI{\\lambda D$$ sliding mode control for hypersonic vehicles with neural network disturbance compensator. *Nonlinear Dyn.* 103 (3). (ISSN:0924-090X). doi:10.1007/s11071-020-06046-y

Tolba, M. F., AboAlNaga, B. D. M., Said, L. A., Madian, A. H., and Radwan, A. G. (2018). Fractional order integrator/differentiator: FPGA implementation and

FOPID controller application. *AEU - Int. J. Electron. Commun.* 98, 220–229. doi:10.1016/j.aeue.2018.10.007

Wachholz, L. C., Valdiero, A. C., and Rasia, L. A. . "Mathematical modeling of a hydraulic motor operated and controlled by proportional valve." COB2019 2019. doi:10.26678/ABCM.COBEM2019.COB2019-2272

Wang, G., Liu, F., Pang, Y., Ren, H., and Ma, Y. (2019). Coal mine intelligence -- the core technical support for the high-quality development of coal industry. *J. coal* 44 (02), 349–357. (ISSN: 0166-5162).

Wang, G., Wang, H., and Ren, H. (2018). Scenario objectives and development path of smart coal mine 2025. *J. coal* 43 (02), 295–305. doi:10.13225/j.cnki.jccs.2018.0152

Wang, H., Wang, J., and Zhang, X. (2020). Theory and technology of integrated and efficient excavation with excavation and anchor. *J. coal* 45 (6), 2021–2030. (ISSN: 0166-5162).

Wu, X., and Huang, Y. (2021). Adaptive fractional-order *non*-singular terminal sliding mode control based on fuzzy wavelet neural networks for omnidirectional mobile robot manipulator - ScienceDirect. *ISA Trans.* 121, 258–267. doi:10.1016/j.isatra.2021.03.035

Yang, Y., Zhao, D-C., Feng, G-L., Geng, D-X., and Guo, H-S. (2022). Energy evolution and acoustic emission characteristics of uniaxial compression failure of anchored layered sandstone. *Front. Earth Sci.* 10, 841598. doi:10.3389/feart.2022.841598

Yin, C., Chen, Y. Q., and Zhong, S. M. (2014). Fractional-order sliding mode based extremum seeking control of a class of nonlinear systems. *Automatica* 50 (3), 3173–3181. doi:10.1016/j.automatica.2014.10.027

Yin, C., Chen, Y. Q., and Zhong, S. M. (2014). Fractional-order sliding mode based extremum seeking control of a class of nonlinear systems. *Automatica* 50 (12), 3173–3181. (ISSN:0005-1098). doi:10.1016/j.automatica.2014.10.027

Zamani, M., Karimi-Ghartemani, M., Sadati, N., and Parniani, M. (2009). Design of a fractional order PID controller for an AVR using particle swarm optimization. *Control Eng. Pract.* 17 (12), 1380–1387. (ISSN:0967-0661). doi:10.1016/j.conengprac.2009.07.005

Zhan, C, Deng, J, and Chen, K (2015). Research on low friction high frequency response variable clearance sealed hydraulic cylinder. *J. Mech. Eng.* 51 (24), 7–5. doi:10.3901/JME.2015.24.161

Zhang, J, and Li, Y (2019). Kinematic error analysis of mechanical arm of roof bolter with uncertain parameters. *J. coal* 44 (10), 3223–3232. (ISSN: 0166-5162).

Zhang, J, Zhang, Q. G., and Zhifu, U (2019). Dynamic uncertainty analysis of mechanical arm of mine roof bolter. *J. coal* 44 (S1), 351–360. (ISSN: 0166-5162).

Zhang, T, Li, G, and Liang, L (2002). Switching variable structure *control* of flexible manipulator with acceleration feedback. *J. Mech. Eng.* 38 (3), 4. doi:10.3321/j.issn:0577-6686.2002.03.009